2015

A parallel dipole line system

Oki Gunawan

Yudistira Virgus

Yudistira Virgus
College of William and Mary

Kong Fai Tai

Recommended Citation

Gunawan, O., Virgus, Y., & Tai, K. F. (2015). A parallel dipole line system. Applied Physics Letters, 106(6), 062407.

A parallel dipole line system

Oki Gunawan,[1,a)] Yudistira Virgus,[1,2] and Kong Fai Tai[3]
[1]*IBM T. J. Watson Research Center, Yorktown Heights, New York 10598, USA*
[2]*Department of Physics, College of William and Mary, Williamsburg, Virginia 23187, USA*
[3]*Division of Physics and Applied Physics, School of Physical and Mathematical Sciences, Nanyang Technological University, 21 Nanyang Link, 637371 Singapore*

(Received 20 November 2014; accepted 23 January 2015; published online 12 February 2015)

We present a study of a parallel linear distribution of dipole system, which can be realized using a pair of cylindrical diametric magnets and yields several interesting properties and applications. The system serves as a trap for cylindrical diamagnetic object, produces a fascinating one-dimensional camelback potential profile at its center plane, yields a technique for measuring magnetic susceptibility of the trapped object and serves as an ideal system to implement highly sensitive Hall measurement utilizing rotating magnetic field and lock-in detection. The latter application enables extraction of low carrier mobility in several materials of high interest such as the world-record-quality, earth abundant kesterite solar cell, and helps elucidate its fundamental performance limitation. © *2015 AIP Publishing LLC*. [http://dx.doi.org/10.1063/1.4907931]

Various matter and particle traps using optical or electromagnetic systems have been developed and instrumental in investigation of many physical phenomena.[1,2] Most macroscale matter trap systems work for spherical or arbitrary shape objects[2] but almost none has been specifically developed for cylindrical objects. This work is initially motivated by the challenge to solve the problem of future electronic integrated circuit fabrication at the end of transistor scaling limit, specifically for semiconductor nanowire (or carbon nanotube) -based integrated circuit.[3–5] One possible route in a "bottom-up" approach is to seek a scalable system that could trap cylindrical objects such as these nanowires into targeted locations for further integrated circuit fabrication.[3,6] Many semiconductor materials are diamagnetic[7] and such materials will be attracted to a region with minimum magnetic field as has been demonstrated in various magnetostatic levitation systems.[8–11] Thus, in principle, it should be possible to design certain magnetic configuration that can trap cylindrical diamagnetic objects.

In this report, we study a unique magnetic trap system for a cylindrical object that can be produced by a parallel dipole line (PDL) system, i.e., a pair of linear distribution of magnetic dipole aligned in parallel, as shown in Fig. 1(a). The system can be experimentally realized using a pair of cylindrical *diametric* magnets, i.e., magnet with magnetization along the diameter.[12] We discovered that a 1D camelback potential naturally arises along the longitudinal direction of the magnet. *This potential is one of the basic model potentials of special interest in physics as it represents a simple confinement potential with two barriers*. We investigate, both theoretically and experimentally, a macroscopic scale prototype utilizing cylindrical diametric magnets and graphite rod as the trapped object and we demonstrate a technique to measure the magnetic susceptibility of the rod. We also report a surprising and yet another important application of the PDL system for high sensitivity Hall measurement that has been used for carrier mobility and density extraction in world-record-quality kesterite solar cell film,[13] a material of current interest in photovoltaics.[14,15]

For a magnetic PDL system, the field distribution at the center plane ($x = 0$) can be described as

$$\mathbf{B}_T(y,z) = \frac{\mu_0 m_L}{2\pi a^2} \sum_{n=1,2} \frac{\bar{w}_n \left[\left(1-\bar{y}^2\right)\left(\bar{y}^2+\bar{w}_n^2\right)+2 \right]}{\left(1+\bar{y}^2\right)^2 \left(1+\bar{y}^2+\bar{w}_n^2\right)^{3/2}} \hat{\mathbf{x}}, \quad (1)$$

where m_L is the dipole moment per unit length, μ_0 is vacuum permeability, a is the half separation between the dipole lines, $\bar{y} = y/a$, $\bar{w}_{1,2} = (L/2 \pm z)/a$, and L is the length of the dipole line (see the supplementary material B.1).[16] The field has only x component due to the symmetry of the system.

A PDL system can be experimentally realized using cylindrical diametric magnet pair (DMP), where the magnetization of the magnet is pointing along the diameter. First, we consider a single DM centered at the origin with length L, radius a, and a uniform magnetization M along x axis:

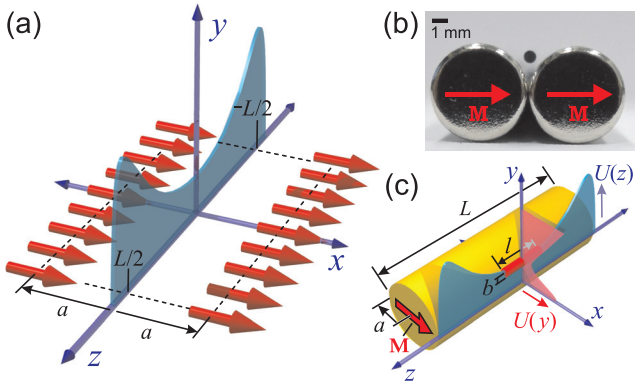

FIG. 1. The PDL system and its experimental realization: (a) The PDL model that produces a camelback potential at the center plane for $|y| < a$. (b) Experimental realization with diametric magnet pair system that serves as magnetic trap for a diamagnetic (graphite) rod. See the supplementary material A (Ref. 16) for detailed system parameters. (c) Schematic diagram of the PDL trap with only one magnet shown.

a)Author to whom correspondence should be addressed. Electronic mail: ogunawa@us.ibm.com

$\mathbf{M} = M\hat{\mathbf{x}}$, as shown in Figs. 1(b) and 1(c). The exact expression for the magnetic field can be derived using magnetic scalar potential model (supplementary material B.2)[16] that yields (in Cartesian vector form [x, y, z])

$$\mathbf{B}_{DM}(x,y,z) = \frac{\mu_0 Ma}{4\pi}\int_0^{2\pi}\sum_{n=1,2}\frac{(-1)^n\cos\phi}{u_n^2+s^2+u_n\sqrt{u_n^2+s^2}} \times\left[x-a\cos\phi, y-a\sin\phi, u_n+\sqrt{u_n^2+s^2}\right]\mathrm{d}\phi \tag{2}$$

where $s^2 = (x-a\cos\phi)^2 + (y-a\sin\phi)^2$ and $u_{1,2} = z \pm L/2$. A pair of these magnets centered at ($\pm$ a,0,0) naturally join and align their magnetizations in the same direction forming a DMP, as shown in Fig. 1(b). The total magnetic field at the center plane is given as: $\mathbf{B}_{T,DMP}(y,z) = \mathbf{B}_{DM}(a,y,z) + \mathbf{B}_{DM}(-a,y,z)$. We refer to this as the DMP model that serves as the exact field calculation model in this work. The PDL model (Eq. (1)) serves as a good approximation for the DMP model especially at the center region (0, y, $z \ll L$), which is often useful as the PDL model provides analytic solutions for most of the equations discussed in this report.

Magnetic Trap for Cylindrical Diamagnetic Object. The PDL system serves as a unique trap for cylindrical diamagnetic object. This can be demonstrated using graphite rod (a strong diamagnetic material) and cylindrical DMP, as shown in Fig. 1(b). We developed theoretical model that describes the confining potentials in all three dimensions that trap the rod (see the supplementary material D–F).[16] We first discuss the vertical confining potential in y-direction at the center ($x=0$, $z=0$), which can be derived from the vertical magnetic field distribution $\mathbf{B}_T(y,0)$ (supplementary material D).[16] To focus on the essential physics, we use long magnet approximation ($L \gg a$) to Eq. (1) which yields

$$\mathbf{B}_{T\infty}(y,0) = \mu_0 M(1-\bar{y}^2)/(1+\bar{y}^2)^2\hat{\mathbf{x}}. \tag{3}$$

We consider a graphite rod with radius b, length l, mass density ρ, and magnetic susceptibility χ trapped at the center plane ($x=0$) [Fig. 1(c)]. A cylindrical rod immersed in this magnetic field will have an induced magnetization (supplementary material C):[16] $\mathbf{M}_R = 2\chi\mathbf{B}_T/\mu_0(2+\chi)$. We assume a small rod radius ($b<a$) so that the magnetic field can be considered uniform over the radial extent of the rod. Since the rod is a diamagnet, the induced magnetization is opposite to the magnetic field and tends to move it towards a region with minimum field and produces levitation or trapping effect.

The equilibrium and stability condition can be investigated by considering the magnetic potential energy of the rod (per unit volume): $U'_M = -\int_0^{B_T}\mathbf{M_R}\cdot d\mathbf{B}$, where $U'_M = U_M/V_R$ with $V_R = \pi b^2 l$ is the rod's volume. The total potential energy, including gravity, is given as: $U'_T = \rho g y + U'_M$, where g is the gravitational acceleration. This potential provides a strong confinement in the vertical direction, illustrated as $U(y)$ in Fig. 1(c). The rod is trapped at potential's minimum at $\bar{y}_0 = y_0/a$, which satisfies

$$\rho g a + \mu_0 M^2\chi/(2+\chi)\times f_Y(\bar{y}_0,\bar{L}) = 0, \tag{4}$$

where $f_Y(\bar{y},\bar{L}) = -a/\mu_0^2 M^2 \times \partial B_T^2(y,z)/\partial y$ is a dimensionless geometrical prefactor function proportional to the diamagnetic repulsion force in y-direction. Using the PDL model (Eq. (1)), we obtain: $f_{Y\infty}(\bar{y}) = 4\bar{y}(3-\bar{y}^2)(1-\bar{y}^2)/(1+\bar{y}^2)^5$ in the long magnet limit ($L \gg a$).

The equilibrium height y_0 can be solved from Eq. (4) if χ is known. Since both the diamagnetic repulsion and the gravity forces are proportional to the rod's volume, y_0 is independent of the rod's radius and length (except for large rod size where the assumption of field uniformity fails). Analysis on the stability at the equilibrium point (supplementary material D) implies the levitation only occurs at y_0 that satisfies: $0.287 < \bar{y}_0 < 1$ with a minimum $|\chi|$ given as: $|\chi|_{\min} = 2/(1+2.069\mu_0 M^2/\rho g a)$. Thus, levitation can be more easily achieved with a rod that has stronger diamagnetic susceptibility and less density; and magnets with stronger magnetization but smaller radius.

One-Dimensional Camelback Potential. The PDL trap system produces a fascinating 1D camelback potential at the center plane that provides a confinement in the z-direction, as illustrated in Fig. 1(a). The camelback hump is associated with the edge effect of the PDL system. For the diamagnetic rod trapped at the center this camelback potential energy (per unit rod volume) can be expressed as

$$U'_M(z) = -\chi/\mu_0(2+\chi)\times B_T^2(y_0,z). \tag{5}$$

Using Eq. (2), we can calculate this potential and the barrier height $\Delta U'_M$, as shown in Figs. 2(a) and 2(b). The camelback peak position can be estimated using PDL model as (supplementary material E):[16] $z_P \simeq \pm(L/2 - \sqrt{2a^2 - y_0^2})$. We can tailor the shape of this camelback potential and the barrier height by tuning the magnet geometrical factor L/a, as shown in Figs. 2(a) and 2(b).

Magnetic Susceptibility Measurement of the Trapped Rod. The dynamics of the trapped rod on the PDL camelback potential can be utilized to measure its magnetic susceptibility. Upon slight disturbance along the z-axis, the rod will execute an oscillation as shown in Fig. 3(a) (see also the video therein) with relatively long oscillation period $T_z \sim 1.4$ s. The underdamped oscillation behavior is attributed to the air friction effect which has negligible effect to the period (<1% error) as long as the damping time constant (τ) satisfies $\tau > T_z$ (the damping practically disappears in

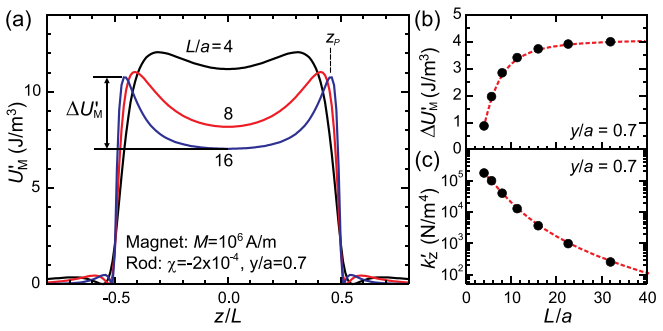

FIG. 2. The camelback potential and its dependence on the magnet's aspect ratio L/a at the center plane ($x=0$). (a) The camelback potential profile for various L/a. $\Delta U'_M$ and z_P are the barrier height and peak position of the camelback hump. (b) The camelback barrier height vs. L/a. (c) The potential "spring constant" k'_z is widely tunable by L/a.

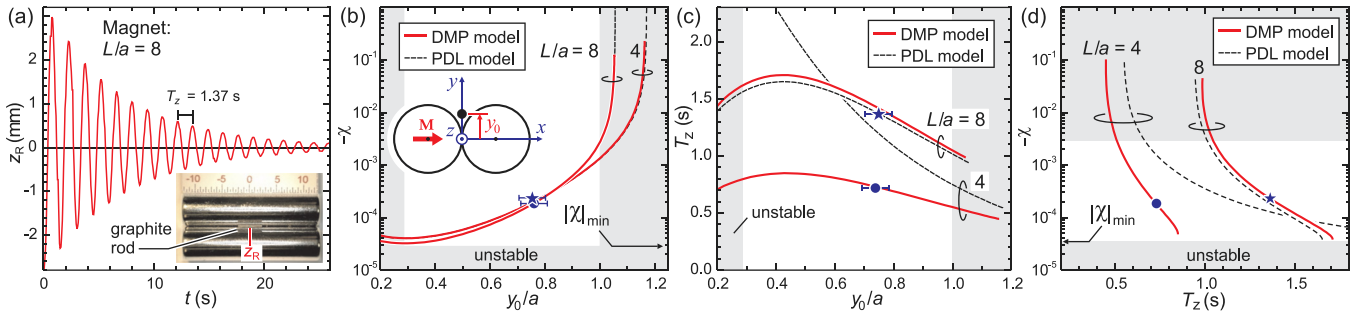

FIG. 3. Magnetic susceptibility determination of a trapped rod: (graphite rod, diameter = 0.55 mm, $l = 4.5$ mm) (a) The rod oscillation on the 1D camelback potential extracted from video (supplementary material A.2).[16] Inset: The oscillation video of the rod. (b) Relationship between rod's χ and the equilibrium height y_0/a using the DMP and PDL models for setup $L/a = 4$ and 8 (see the supplementary material A.1).[16] Experimental data point are shown as star (circle) for $L/a = 8$ (4) with χ determined from Fig. 3(d). Shaded regions indicate unstable or no levitation for $L/a = 8$ setup. (c) Relationship between period T_z vs. y_0/a and the experimental data. (d) Relationship between χ vs. T_z and the experimental data. (Multimedia view) [URL: http://dx.doi.org/10.1063/1.4907931.1]

vacuum as shown in the supplementary material H).[16] To analyze the oscillation we assume a small rod radius ($b \ll a$), short rod approximation ($l \ll L$), and small oscillation amplitude ($z \ll L$) so that the camelback potential at the center can be well approximated by a parabolic potential: $\Delta U_z'(z) = \frac{1}{2}k_z' z^2$. Here, $k_z' = \partial^2 U_T'(0, y_0, 0)/\partial z^2$ is the harmonic potential "spring constant" (per unit rod's volume) given as

$$k_z' = -\mu_0 M^2 \chi/(2+\chi) \times f_{Z2}(\bar{y}_0, \bar{L})/L^2, \tag{6}$$

where $f_{Z2}(\bar{y}, \bar{L}) = L^2/\mu_0^2 M^2 \times \partial^2 B_T^2(y, 0)/\partial z^2$ is a dimensionless geometrical prefactor function for k_z'. It can be calculated exactly using the DMP model (Eq. (2)) or approximately using the PDL model (Eq. (1)) that yields (supplementary material G):[16] $f_{Z2}(\bar{y}, \bar{L}) = 96\bar{L}^4(\bar{L}^2 + 4\bar{y}^2 - 16)[8 + (\bar{L}^2 + 4\bar{y}^2)(1 - \bar{y}^2)] / [(1+\bar{y}^2)^2(4 + \bar{L}^2 + 4\bar{y}^2)^5]$. This "spring constant" k_z' can be widely tuned by the magnet aspect ratio L/a, e.g., by a factor of 10^{-3} by changing L/a from 4 to 40 [Fig. 2(c)].

The oscillation period for the trapped rod can be expressed as: $T_z = 2\pi\sqrt{\rho/k_z'}$. This leads to an interesting outcome where by measuring T_z, we could determine the rod's magnetic susceptibility given as

$$\chi = -2/(1 + \mu_0 M^2 f_{Z2}(\bar{y}_0, \bar{L}) T_z^2/4\pi^2 \rho L^2). \tag{7}$$

Note that here we need to know y_0. Surprisingly, T_z is directly related to y_0 only by the geometrical factors of the magnet (L and a) and independent of the magnet's M and the property of the rod (χ, ρ, b, and l) (see the supplementary material G).[16] This relationship is given below and plotted in Fig. 3(c)

$$T_z = f_T(\bar{y}_0, \bar{L}) = 2\pi\sqrt{L^2 f_Y(\bar{y}_0, \bar{L})/g\, a\, f_{Z2}(\bar{y}_0, \bar{L})}. \tag{8}$$

Therefore, to determine χ of the rod, we first measure T_z, solve for $\bar{y}_0$, i.e., $y_0 = f_T^{-1}(T_z, \bar{L})$ and then use Eq. (7). We illustrate the χ measurement in two PDL trap setups (supplementary material A)[16] with aspect ratio: $L/a = 4$ and 8 but the same radius ($a = 3.2$ mm) using a short graphite rod, as presented in Fig. 3. We provide two calculation models: "exact" using the DMP (Eq. (2)) model and "approximation" using the PDL model (Eq. (1)). First, we measure T_z and y_0 then plot the data points in Fig. 3(c). We also plot the expected T_z vs. y_0 curves from Eq. (8). We observe good agreement between the data and the DMP model for both magnet setups. Therefore, given T_z we could also determine y_0 without measuring it.

Next, we determine χ from Eq. (7) using the DMP model, as plotted in Fig. 3(d). Measurements from both setups yield good agreement, i.e., $\chi = -(2.20 \pm 0.32) \times 10^{-4}$ and $\chi = -(1.80 \pm 0.38) \times 10^{-4}$ for setup $L/a = 8$ and 4, respectively, indicating the consistency of our model. Note that these results are within the reported χ value for graphite in literature: $\chi_\perp = -1.4 \times 10^{-5}$ and $\chi_\parallel = -6.1 \times 10^{-4}$ for χ measured along perpendicular and parallel to the c-axis, respectively.[17] Our graphite rod is amorphous thus its χ should be a mixture of both χ orientations.

One could also determine χ from y_0, as illustrated in Fig. 3(b), however, T_z measurement is easier and more accurate (unlike the error bar for y_0, the error bar for T_z is small and not visible in Fig. 3). Figs. 3(b)–3(d) also show that the PDL model becomes closer to the DMP model for long magnet case ($L/a \gtrsim 5$). This is reasonable as the magnet becomes longer the PDL model becomes a better approximation to the DMP model at the center of the trap (see the supplementary material B.3).[16] The technique described here provides an alternative and simpler χ measurement for diamagnetic (cylindrical) material compared to existing technique such as vibration sample magnetometer.[18]

High Sensitivity Hall Measurement with Rotating PDL System. The PDL system has another important application for high sensitivity Hall measurement of semiconductor materials with low carrier mobility ($\mu \lesssim 1$) cm^2/Vs), low carrier density, or very thin film that yields very high sheet resistance ($R_S \gtrsim 10$ MΩ/sq). To obtain successful Hall measurement, the ratio between the transverse (R_{xy}) and longitudinal (R_{xx}) resistance: $R_{xy}/R_{xx} = B\mu$ has to be sufficiently large ($\gtrsim 10^{-4}$). This can be achieved in high carrier mobility samples or using very high magnetic field (B). The conventional static (dc) field Hall measurement of R_{xy} on these insulating samples is often unreliable due to large noise and large drifting background coming from some R_{xx} contribution. Nevertheless, one can improve the Hall measurement signal to noise ratio using oscillating (ac) magnetic field system and lock-in detection scheme.[19,20]

The PDL system, realized using cylindrical DMP system, has the ideal features to perform lock-in detection of

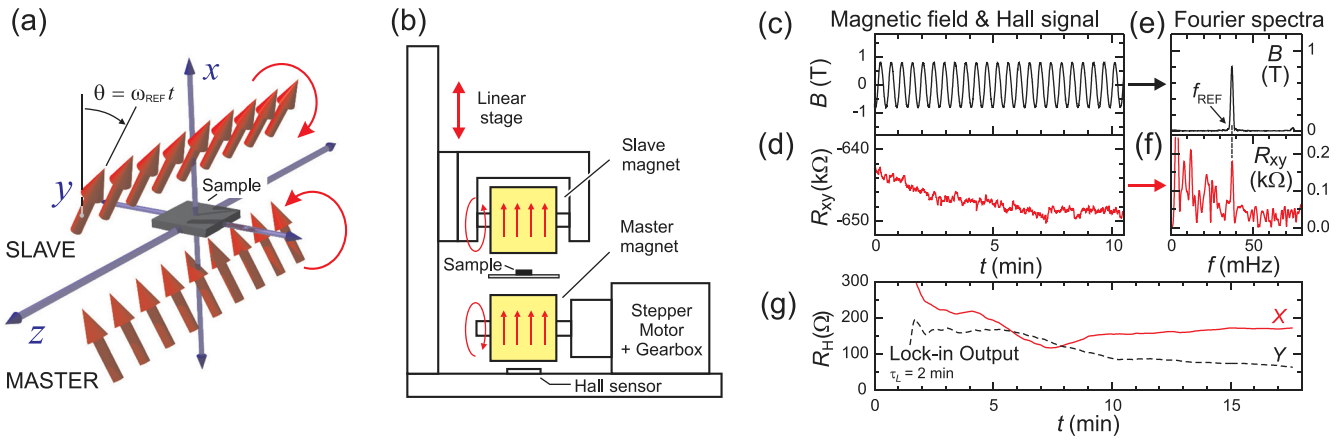

FIG. 4. High-sensitivity Hall measurement with rotating PDL system on a world-record-quality kesterite solar cell film: (a) Experimental concept showing rotating PDL in master-slave configuration. (b) Experimental setup using cylindrical DMP. (c) Magnetic field B at the sample vs. time, deduced from the Hall sensor placed at the bottom. (d) Transverse resistance R_{xy} from "CZTSSe-1" Van der Pauw sample. (e) Fourier spectra of B. (f) Fourier spectra of R_{xy}. (g) Numerical lock-in output of R_{xy} showing the in-phase component (X) as the desired Hall signal and the out-of-phase component (Y) which comes from the parasitic emf voltage.

Hall signal. Due to coupling between the two dipole lines, a rotation in one dipole line will be mirrored by the other, as shown in Fig. 4(a). This allows a simple master-slave configuration that doubles the field and makes it unidirectional at the center. The master magnet is driven by a motor and the rotation is mirrored by the slave magnet, as shown in Fig. 4(b). Our standard setup uses cylindrical DMP with: $a = 12.7$ mm, $L = 25.4$ mm, and $M = 10^6$ A/m and gap separation of ~5 mm between the magnets' surface. The sample (a van der Pauw type $\sim 5 \times 5$ mm) is placed at center. This system has several favorable characteristics for lock-in ac Hall measurement such as: (1) Unidirectional field (in x-direction) with excellent uniformity on the sample (e.g., only ~2% standard deviation for 5×5 mm sample). (2) Strong magnetic field at the center (~1.9 T peak-to-peak). (3) High purity single harmonic magnetic field oscillation, which is important to avoid higher harmonics content in the Hall signal that will otherwise complicate the data interpretation. (4) Compact and low cost.

This system was developed to extract the hole mobility in kesterite ($Cu_2ZnSn(S,Se)_4$ or CZTSSe) solar cell,[21] where conventional dc field Hall system was unsuccessful (due to its low mobility). The characterized films have similar quality and performance (power conversion efficiency $\eta \sim 12\%$) with the recent world-record IBM CZTSSe solar cell ($\eta = 12.6\%$).[13] However, this efficiency is still far below the more well-established $Cu(In,Ga)Se_2$ (CIGS) solar cell ($\eta = 20.8\%$)[22] and prompts further investigation.

An example of the rotating PDL Hall measurement on "CZTSSe-1" sample is shown in Fig. 4(b). The master magnet is driven by the motor at a constant angular speed, while the Hall sensor (at the bottom) measures the field that serves as the reference rotation signal. The magnetic field at the sample was deduced and plotted in Fig. 4(c). The signal shows a dominant Fourier component at f_{REF} as expected [Fig. 4(e)]. The transverse resistance R_{xy} signal was concurrently recorded [Fig. 4(d)]. The signal looks noisy with large and drifting background which often occurs in highly resistive or low mobility sample. Nevertheless, the Fourier spectrum of the signal (after a polynomial background subtraction) [Fig. 4(f)] shows a significant peak at the same frequency f_{REF} suggesting the existence of the desired Hall signal (there is also a typical background "1/f" noise that becomes more dominant at lower frequency). Subsequently, we perform *numerical* lock-in detection on R_{xy} [Fig. 4(g)] to separate the in-phase or the desired Hall signal component (X) from the out-of-phase parasitic component (Y) due to emf voltage induced by the oscillating magnetic flux. The operating f_{REF} is restricted at low frequency (~40 mHz) to minimize the parasitic emf signal Y. This condition dictates the use of long lock-in time constant ($\tau_L = 2$ min). We observe a steady lock-in output for X after $5\tau_L$ that yields the final Hall signal $R_H = 172\ \Omega$ (positive sign indicates a p-type carrier as expected), which is 3800× smaller than the background R_{xy} (~650 kΩ) [Fig. 4(d)]. This example highlights the problem in the conventional static field Hall measurement and demonstrates the efficacy of the rotating PDL Hall system. This measurement yields carrier density $p = 1.6 \times 10^{16}/\text{cm}^3$ and mobility $\mu_h = (0.31 \pm 0.05)$ cm^2/Vs (see Table S2 in supplementary material I for more detail).[16]

Using this technique, we have extracted the hole mobility and carrier density of several (~10) champion grade CZTSSe films and compare them with CIGS samples of similar efficiency ($\eta \sim 9 - 12\%$). We consistently observe the expected Hall signal Fourier component at f_{REF}, as shown in supplementary material I,[16] the signal becomes cleaner and easier to detect with higher mobility as expected. The measurements yield average CZTSSe hole mobility: $\mu_h = (0.5 \pm 0.1)$ cm^2/Vs, which is significantly lower than that of CIGS: $\mu_h = (4 \pm 0.4)$ cm^2/Vs. The lower mobility in CZTSSe leads to lower bulk conductivity and sheds some light to its fundamental issue such as higher series resistance, lower fill factor (see Table I in Ref. 13), and the Voc pinning behavior in Suns-Voc curve at high light intensity.[23] Lower mobility is also often associated with higher disorder in the material and consistent with more severe band tail states in CZTSSe.[24] This rotating PDL Hall system has also been used to perform Hall measurement in other low mobility, very thin or very insulating materials such as CdS and Zn(O,S)[25] (see also supplementary material I)[16] and has

been routinely used to monitor carrier density of the CZTSSe films for device optimization.

We thank Chang Tsuei and Qing Cao (IBM) and Andika Putra (University of Maryland) for review. O.G. conceived and executed the project. Y.V. worked on the PDL trap and K.F.T. worked on the rotating PDL Hall system. For the CZTSSe study, the information, data, or work presented herein was funded in part by the U.S. Department of Energy, Energy Efficiency and Renewable Energy Program, under Award Number DE-EE0006334, see the supplementary material[16] for more information; it was also part of a joint development project between Tokyo Ohka Kogyo Co., Ltd., Solar Frontier K. K. and IBM Corporation. K.F.T. acknowledges support from Energy Research Institute at NTU (ERI@N) and Clean Energy Program Office, National Research Foundation of Singapore.

[1]W. Paul, Rev. Mod. Phys. **62**, 531 (1990).
[2]A. Ashkin, IEEE J. Quantum Electron. **6**, 841 (2000).
[3]D. Whang, S. Jin, Y. Wu, and C. M. Lieber, Nano Lett. **3**, 1255 (2003).
[4]J. Appenzeller, J. Knoch, M. Bjoerk, H. Riel, H. Schmid, and W. Riess, IEEE Trans. Electron Devices **55**, 2827 (2008).
[5]S. J. Kang, C. Kocabas, T. Ozel, M. Shim, N. Pimparkar, M. A. Alam, S. V. Rotkin, and J. A. Rogers, Nat. Nanotechnol. **2**, 230 (2007).
[6]R. Agarwal, K. Ladavac, Y. Roichman, G. Yu, C. Lieber, and D. Grier, Opt. Express **13**, 8906 (2005).
[7]D. J. Chadi, R. M. White, and W. A. Harrison, Phys. Rev. Lett. **35**, 1372 (1975).
[8]A. K. Geim, M. D. Simon, M. I. Boamfa, and L. O. Heflinger, Nature **400**, 323 (1999).
[9]M. D. Simon and A. K. Geim, J. Appl. Phys. **87**, 6200 (2000).
[10]I. F. Lyuksyutov, D. G. Naugle, and K. D. D. Rathnayaka, Appl. Phys. Lett. **85**, 1817 (2004).
[11]G. Kustler, Rev. Roum. Sci. Techn. –Électrotechn. et Énerg. **52**, 265 (2007).
[12]O. Gunawan and Q. Cao, "Magnetic trap for cylindrical diamagnetic materials," U.S. patent 8,895,355 (25 November 2014).
[13]W. Wang, M. T. Winkler, O. Gunawan, T. Gokmen, T. K. Todorov, Y. Zhu, and D. B. Mitzi, Adv. Energy Mater. **4**, 1301465 (2014).
[14]D. B. Mitzi, O. Gunawan, T. K. Todorov, K. Wang, and S. Guha, Sol. Energy Mater. Sol. Cells **95**, 1421 (2011).
[15]K. Ito, *Copper Zinc Tin Sulfide-Based Thin Film Solar Cells* (John Wiley and Sons, 2014).
[16]See supplementary material at http://dx.doi.org/10.1063/1.4907931 for more details.
[17]N. Ganguli and K. S. Krishnan, Proc. R. Soc. London, Ser. A **177**, 168 (1941).
[18]S. Foner, Rev. Sci. Instrum. **30**, 548 (1959).
[19]N. Z. Lupu, N. M. Tallan, and D. S. Tannhauser, Rev. Sci. Instrum. **38**, 1658 (1967).
[20]O. Gunawan and T. Gokmen, "Hall measurement system with rotary magnet," U.S. patent application 13/568,627 (27 July 2012).
[21]Standard CZTSSe and CIGS films were synthesized on Mo-coated glass, they were subsequently exfoliated away from the Mo layer to a secondary substrate for Hall measurement to prevent shunting.
[22]P. Jackson, D. Hariskos, R. Wuerz, W. Wischmann, and M. Powalla, Phys. Status Solidi RRL **8**, 219 (2014).
[23]O. Gunawan, T. Gokmen, and D. B. Mitzi, J. Appl. Phys. **116**, 084504 (2014).
[24]T. Gokmen, O. Gunawan, T. K. Todorov, and D. B. Mitzi, Appl. Phys. Lett. **103**, 103506 (2013).
[25]H. H. Park, A. Jayaraman, R. Heasley, C. Yang, L. Hartle, R. Mankad, R. Haight, D. Mitzi, O. Gunawan, and R. G. Gordon, Appl. Phys. Lett. **105**, 202101 (2014).